Performance of Multiplexed XY Resistive Micromegas detectors in a high intensity beam

D. Banerjee [l], V. Burtsev [j], A. Chumakov [j], D. Cooke [l], E. Depero [l], A.V. Dermenev [e],
S.V. Donskov [i], F. Dubinin [f], R.R. Dusaev [j], S. Emmenegger [l], A. Fabich [d], V.N. Frolov [b],
A. Gardikiotis [h], S.N. Gninenko [e], M. Hösgen [a], A.E. Karneyeu [e], B. Ketzer [a], M.M. Kirsanov [e],
I.V. Konorov [c,f], V.A. Kramarenko [g], S.V. Kuleshov [k], E. Levchenko [j], V.E. Lyubovitskij [j,k],
V. Lysan [b], S. Mamon [j], V.A. Matveev [b], Yu.V. Mikhailov [i], V.V. Myalkovskiy [b],
V.D. Peshekhonov [b,1], D.V. Peshekhonov [b], V.A. Polyakov [i], B. Radics [l], A. Rubbia [l],
V.D. Samoylenko [i], V.O. Tikhomirov [f], D.A. Tlisov [e], A.N. Toropin [e], B. Vasilishin [j],
G. Vasquez Arenas [k], P. Ulloa [k], P. Crivelli [l,*]

[a] *Universität Bonn, Helmholtz-Institut für Strahlen-und Kernphysik, 53115 Bonn, Germany*
[b] *Joint Institute for Nuclear Research, 141980 Dubna, Russia*
[c] *Technische Universität München, Physik Department, 85748 Garching, Germany*
[d] *CERN, European Organization for Nuclear Research, CH-1211 Geneva, Switzerland*
[e] *Institute for Nuclear Research, 117312 Moscow, Russia*
[f] *P.N. Lebedev Physics Institute, Moscow, Russia, 119 991 Moscow, Russia*
[g] *Skobeltsyn Institute of Nuclear Physics, Lomonosov Moscow State University, Moscow, Russia*
[h] *Physics Department, University of Patras, Patras, Greece*
[i] *State Scientific Center of the Russian Federation Institute for High Energy Physics of National Research Center 'Kurchatov Institute' (IHEP), 142281 Protvino, Russia*
[j] *Tomsk Polytechnic University, 634050 Tomsk, Russia*
[k] *Universidad Técnica Federico Santa María, 2390123 Valparaíso, Chile*
[l] *ETH Zurich, Institute for Particle and Astrophysics, CH-8093 Zurich, Switzerland*

ARTICLE INFO

ABSTRACT

We present the performance of multiplexed XY resistive Micromegas detectors tested in the CERN SPS 100 GeV/c electron beam at intensities up to 3.3×10^5 $e^-/(s \cdot cm^2)$. So far, all studies with multiplexed Micromegas have only been reported for tests with radioactive sources and cosmic rays. The use of multiplexed modules in high intensity environments was not explored due to the effect of ambiguities in the reconstruction of the hit point caused by the multiplexing feature. For the specific mapping and beam intensities analyzed in this work with a multiplexing factor of five, more than 50% level of ambiguity is introduced due to particle pile-up as well as fake clusters due to the mapping feature. Our results prove that by using the additional information of cluster size and integrated charge from the signal clusters induced on the XY strips, the ambiguities can be reduced to a level below 2%. The tested detectors are used in the CERN NA64 experiment for tracking the incoming particles bending in a magnetic field in order to reconstruct their momentum. The average hit detection efficiency of each module was found to be ~96% at the highest beam intensities. By using four modules a tracking resolution of 1.1% was obtained with ~85% combined tracking efficiency.

* Corresponding author.
  E-mail address: crivelli@phys.ethz.ch (P. Crivelli).
[1] Deceased.

1. Introduction

In the past years, a lot of effort has been invested in the development of microstrip gas detectors for particle tracking in various experiments (e.g [1]). Among those, Micromegas (MICRO-MEsh GASeous Structure) [2] have found many applications in particle [3], nuclear [4] and astrophysics [5] for the detection of ionizing particles. This relatively high-gain ($\sim 10^4$) gas detector combines excellent spatial accuracy with a resolution below 100 μm [6], robustness, high rate capabilities, good timing resolution (<100 ns) and low material budget. Furthermore, this technology found applications in fire detectors [7] and muon tomography of volcanoes and pyramids [8].

Various improvements to this detector technology have continued since its first conception to make it more functional for applications in basic and applied research. One of such developments was the introduction of resistive strips to limit the current in case of a discharge and, thus, reduce the deadtime allowing Micromegas to operate in high flux environments [9]. Several resistive Micromegas chambers with two-dimensional readout have been tested in the context of R&D work for the ATLAS Muon system upgrade [10].

The need of experiments to have large scale tracking detectors with good spatial resolution is constantly growing. This implies a small strip pitch and hence a large number of readout channels. In order to make this more cost effective, an innovative technique for the readout, called genetic multiplexing, was developed to connect multiple strips to individual readout channels thus reducing the required number of channels [11]. However, this grouping leads to larger detector capacitance, especially for large scale detectors, and thus limit the S/N ratio. Also fake combinations of "ghost" clusters are expected especially for high particle fluxes when pile-up is more likely. This technology has only been tested for cosmic ray events [12] until now and studies are required to assess its extension to larger scale systems under higher flux.

In this paper we present the first measurements with resistive XY Micromegas modules multiplexed by a factor of five in a high particle flux. This test was done using the CERN SPS H4 high intensity secondary beamline in the context of the NA64 experiment [13]. Our results show that fake combinations can be suppressed very efficiently by using the additional information of cluster size and integrated charge of signal clusters. The experimental setup and the description of the Micromegas modules is presented in the following sections along-with its performance results.

2. NA64

The CERN NA64 experiment combines the active beam dump technique with missing energy measurement searching for invisible decays of massive A' produced in the reaction:

$$e^- Z \rightarrow e^- Z A' \tag{1}$$

of electrons scattering off a nuclei of mass number Z, with a mixing strength $10^{-6} < \epsilon < 10^{-3}$ and masses $M_{A'}$ in the sub-GeV range [14]. The secondary beam is produced by dumping the SPS 400 GeV protons at the Fixed Target T2 of the CERN North Area. The electrons are then transported to the detector in the evacuated H4 beamline tuned to a freely adjustable beam momentum from 10 up to 300 GeV/c. The detailed setup of the experiment is shown in Fig. 1.

The 100 GeV/c electron beam entering the setup is triggered by the coincidence of scintillators S1–S3. The typical maximal beam intensity used for NA64 is of the order of 5×10^6 e^- for a SPS spill with 10^{12} protons on target [16]. Each spill has a duration of 4.8 s and the beam has a diameter ~ 2 cm (FWHM). The maximal beam intensity thus achieved is $\sim 3.3 \times 10^5$ e^-/(s cm^2). The beam is dumped on the electromagnetic calorimeter (ECAL), a sandwich of lead and scintillators (corresponding to $40 X_0$ where X_0 is the radiation length), to produce massive A' through scattering with the heavy nuclei. In case of a A' production, a fraction of the energy (the chosen threshold of the

experiment is $0.5 \cdot E_0$ where E_0 is the beam energy) will be deposited in the ECAL and the rest will be carried away by the A' without any interaction downstream of the ECAL. The signature for a signal will be missing energy in the ECAL and no activity in the VETO (V2, three plastic scintillator planes) and the four hadronic calorimeter modules (HCAL 1–4, a sandwich of iron and scintillators). The main sources of background for this search come from

1. electrons in the low energy tail of the beam mistaken as a high energy one depositing all its energy in the ECAL,
2. hadron contamination in the electron beam producing neutrals that carry away an energy larger than the ECAL threshold,
3. muons producing a low energy photon or delta electron with energy smaller than $0.5 \cdot E_0$ in the ECAL, which is absorbed in the calorimeter while the muon penetrates the rest of the detector without being detected.

A detailed description of all the expected background sources is presented in [13]. Beam hadrons and muons are suppressed at a level of 10^{-5} by tagging the synchrotron radiation of the incoming particles deflected in the magnetic field [17]. To suppress low energy electrons, a spectrometer is required for NA64 to track the incoming particles and reconstruct their momentum in a magnetic field [18]. Any charged particle with momentum p entering a magnetic field, B, is deflected by the field with the curvature radius of the trajectory $r = p/(qB)$, where q is the charge of the particle. Four Multiplexed XY Resistive Micromegas detectors (MM1–MM4) were built for this reconstruction. The magnetic field used during the experiment is ~ 7 T.m in a 4.8 m long magnet. Two modules were positioned before the magnet ~ 1 m apart and two downstream ~ 13 m from the end of the magnet before the ECAL. MM3 and MM4 were placed ~ 1.5 m from each other (see Fig. 1).

3. The micromegas modules

3.1. Principle of operation

Micromegas detectors are two-stage parallel plate avalanche chambers with a narrow amplification gap and a wider drift gap as shown in the right picture of Fig. 2. Our modules have a drift gap of 5 mm separated from the amplification gap by a Nickel electro-formed micro-mesh. The drift cathode is made of a copper mesh and the amplification gap of 128 μm is defined by photo-resistive pillars 300 μm in diameter, equally spaced by 5 mm. The amplification mesh is formed of 400 wires (per inch) with an aperture size ~ 45 μm and wire diameter ~ 18 μm. The thickness of the mesh is ~ 29 μm. The gas chambers are filled with mixtures of Ar and a quenching gas. A charged particle entering the detector ionizes the gas producing electrons that drift towards the micro-mesh under the electric field of the drift cathode, ~ 0.6 kV/cm, wherein they enter the amplification region producing an avalanche of secondary electrons under the high amplification field ~ 50 kV/cm. The signal induced on the X and Y strips is read by the front-end chips.

The electrons produced in the amplification gap can also cause excitation of the gas molecules which return to the ground state via emission of UV photons [19,20]. These UV photons can release new electrons from the gas molecules by photo-electric effect and eventually result in detector breakdown. Therefore, molecular gases with absorption bands in the UV range [21,22] are mixed with a noble gas (7% CO_2 with 93% Ar in our case) to act as a "quencher" to absorb these UV photons.

3.2. Design of NA64 Micromegas detectors

The results from the R&D work performed for the ATLAS Muon System upgrade [10] on several 2D Micromegas chambers with spark protection guided our design of the strip widths and pitch for the NA64 modules. Our resistive detectors were produced at the CERN EP-DT-EF workshop. The readout strips are multiplexed by a factor five and the resistive strips (R strips) of resistance 50 MΩ/cm are placed parallel to
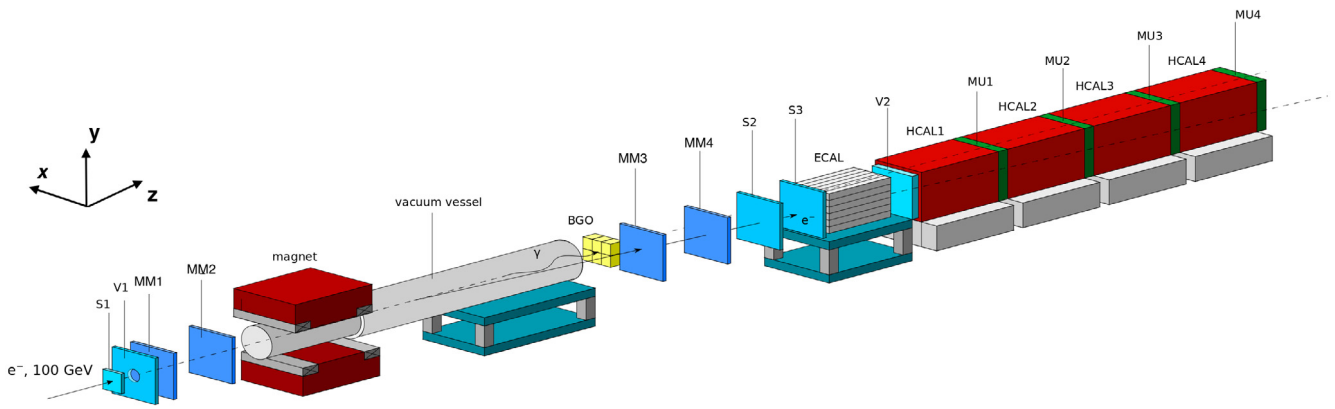
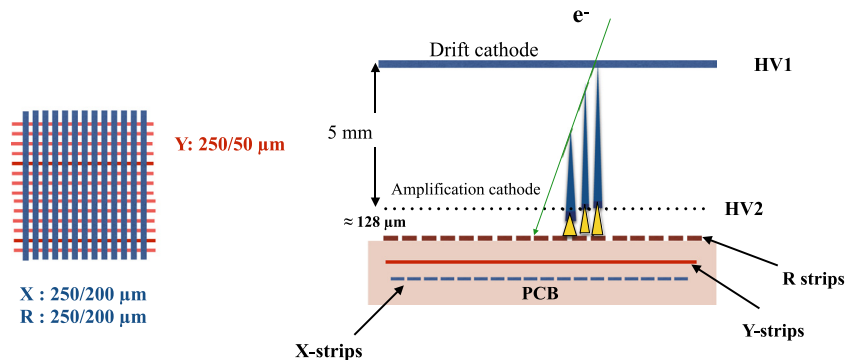**Fig. 1.** NA64 detailed setup showing all sub-detectors (taken from [15]).

Fig. 2. Left: Sketch of the strip dimensions of the Micromegas modules. The pitch of the strip layers is 250 μm. Right: Principle of operation of a Micromegas detector.
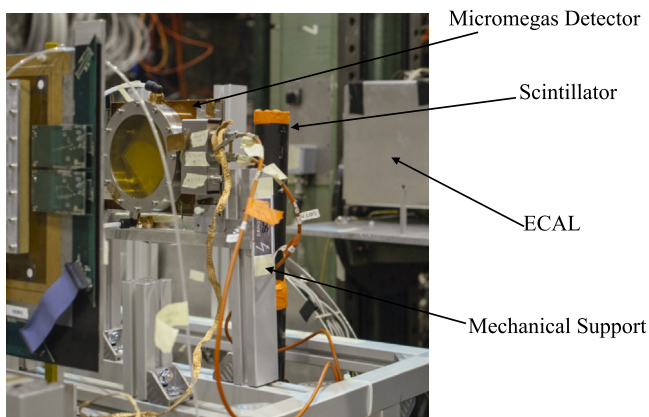

Fig. 3. Micromegas detector placed in the CERN SPS H4 beam line.

the X-strips as shown in the left picture of Fig. 2. The R and X strips have the same width of 200 μm with the Y strips placed below the R strips and perpendicular to the X-strips with a width of 50 μm. The pitch of the strips in all layers is 250 μm. The active detector area is 8 cm × 8 cm, with 320 strips each for the X and Y coordinates. The readout is done with a 128 channel APV chip [23] as for the COMPASS GEM and Micromegas detectors [24]. A multiplexing factor of five allows to have one chip per detector to read all 640 strips. Fig. 3 shows one of the Micromegas modules installed at the CERN SPS H4 beam line.

The rotation with respect to the average beam axis and the position of the modules was known to a precision ~±0.5° and ±1 mm respectively. Any misalignment of the modules and the precision of the

orientation with respect to the beam axis was not taken into account for the estimation of the spatial resolution as described below.

3.3. Multiplexing

The genetic multiplexing algorithm [11] exploits the fact that a single particle entering the detector produces isolated tracks. The detected hits therefore occupy only a few neighboring readout strips in a small area. This allows to group several strips to single electronic channels, thus reducing the required number of channels and, therefore, the cost of electronics. In this mapping construction there is only one set of two consecutive strips corresponding to a given set of two electronic channels. Using this scheme the theoretical number of readout strips that can be read by p electronic channels is given by the maximum number of unordered doublets as

$$n_{max} = \frac{p \times (p-1)}{2} + 1 \quad p = \text{odd}$$

$$n_{max} = \frac{p \times (p-2)}{2} + 2 \quad p = \text{even}.$$

Therefore in principle the maximum number of strips that can be multiplexed to be read by the 128 channel APV chip is ~ 8000. For the NA64 modules this multiplexing factor was reduced to five (corresponding to 640 strips per module) in order to limit ambiguities expected at high intensities. The multiplexing formula used to obtain the channel-strip ($c(s)$) mapping per plane where $c(s)$ is the channel corresponding to strip s is:

$$c(s) = \text{mod } (s \times (\text{floor}(s/p) \times m + 1), p) \qquad (2)$$

where p is the number of electronic channels = 64, $m = 6$ and mod and floor are the modulo and the rounding down functions. The variable, m, gives the maximum cluster size which does not lead to repetition of at least two consecutive strip connections. The above equation is, however, only valid when p and $m + 1$ does not share a common prime factor.
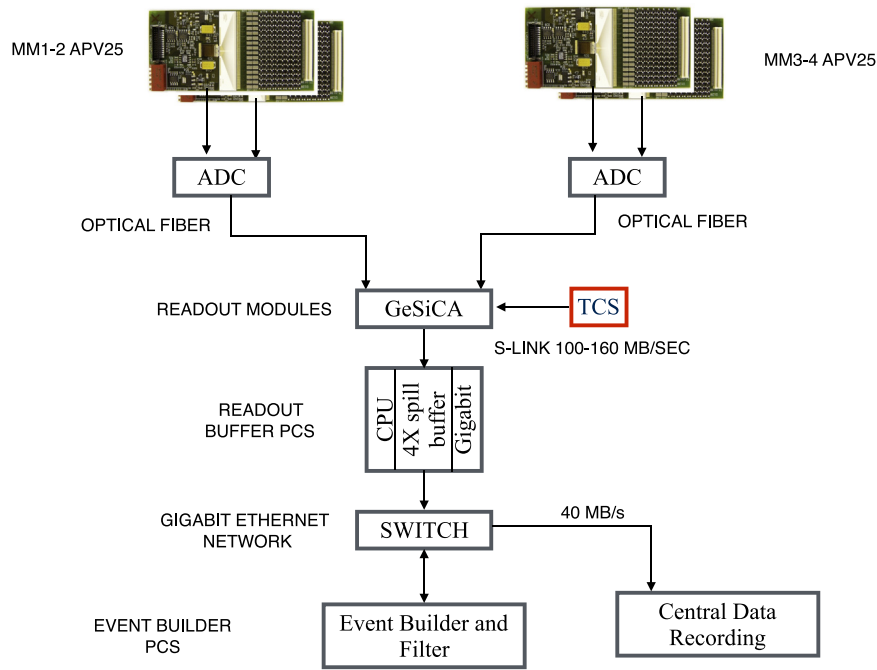
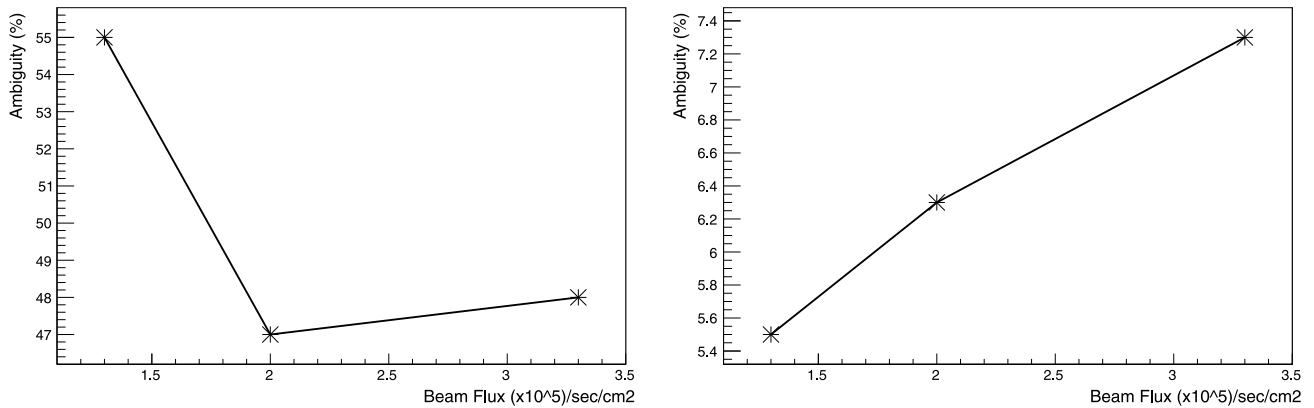**Fig. 4.** General schematic of the NA64 DAQ.

Fig. 5. Probability of ambiguity (%) due to cluster signal spread estimated for one-particle-hit events (left) and due to pileup events for two-particle-hit events (right).

3.4. Signal cluster reconstruction

When the trigger from the experiment is received, the APV25 chips output for each channel three analog charge samples separated by 25 ns. Those signals are digitized by the ADC and are read by the common DAQ [25] of the experiment as shown in the general schematic of Fig. 4. The pedestal distribution of the electronic channels, obtained from the average of the three charge samples/channel, are recorded in absence of the beam. The noise is defined as the RMS fluctuation (sigma) of each channel around its pedestal. The latency is set such that the three samples lie on the rising edge of the signal with the third sample closest to the peak. A hit on a strip is defined when the third sample is at least three sigma above the pedestal level. The maximum of the three samples is then recorded as the charge information of the hit strip. When a charged particle enters the detector, it ionizes the gas and, therefore, a signal on consecutive strips is expected due to the drift of the ionized electrons in the gas volume and the consequent charge spread. A signal cluster is defined when at least two neighboring strips are hit. To reconstruct the position of a signal cluster, the electronic channels are mapped to the multiplexed strips. The hit position on each plane (X and

Y) is calculated by weighting the strip positions with the corresponding charges recorded on the strips.

The multiplexing of the modules can cause some ambiguities in the signal reconstruction due to loss of information. In fact if two particles enter the detector at the same time different combinations of channels may arise giving "ghost" signal clusters. Smaller "ghost" clusters with two or more strips may also arise if a signal cluster has a large spread (>6 strips). For example in our design, the $channel_{strip}$ combination for channels 0 and 7 are given by: 0_0 0_{64} 0_{128} 0_{192} 0_{256} and 7_7 7_{65} 7_{163} 7_{253} 7_{287}. Channels 0–7 are also connected to strips 0–7 apart from its other connections. So for a 7-strip wide signal cluster (not unlikely as will be shown in the following Section) between strips 0 and 7, the connection of channels 0 and 7 to the consecutive strips 64 and 65 will give rise to a fake combination and produce a "ghost" cluster.

Here we show that one can substantially suppress these "ghost" clusters by using the information from the integrated charge of the cluster and its size as proposed in [11]. By listing all possible signal clusters on each plane that share the same readout channel, the cluster with the largest number of strips and with largest integrated charge is selected. In fact, all the others are results of fake combinations rather than real particle hits.
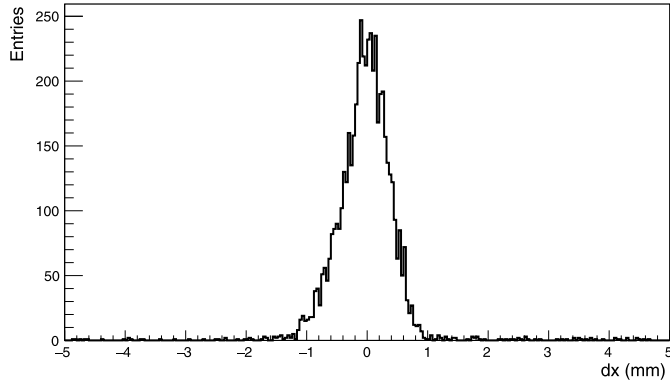
Fig. 6. Distribution of difference of the cluster positions in each projection between MM 3 and 4 after selecting parallel tracks within the beam spot with MM 1 and 2 with energy 100 GeV ± 2 GeV selected with the ECAL.
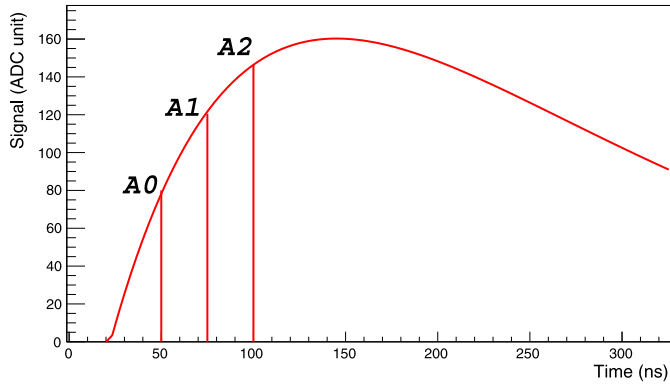

Fig. 7. Shape of signal sampled by a APV chip indicating the three samples 25 ns apart.

In order to estimate the level of ambiguity due to the spread of signal clusters larger than six strips, we compared one-particle-hit events before and after the cleaning. Fig. 5 (left) shows the fraction of events that were wrongly identified as having more than one cluster for one particle hit before the cleaning as a function of the beam flux. As expected there is no correlation between this probability and the beam flux.

To estimate the ambiguity due to pile up of particles, two-particle-hit events are compared before and after the cleaning. Almost 80% of the two-particle-hit events give more than two signal clusters before the cleaning. Since, the fraction of two-particle-hit events range between 7% and 9% of the total events depending on the flux, the probability of ambiguity due to the pile up is around 5%–7% for ∼100 kHz/(s cm²) beam flux, as shown on the right side of Fig. 5.

To estimate the level at which a "ghost" cluster was selected instead of the true signal cluster, with the method described above, we compared the position of the signal clusters on MM 3 and MM 4 for a deflected beam under the magnetic field ∼ 7 T.m. A parallel incoming track was selected within the beam spot using the position information from MM 1 and 2 such that its energy in the ECAL was in the range 100 GeV ± σ_{ECAL} where σ_{ECAL} ∼2 GeV is the energy resolution of the ECAL. Fig. 6 shows the distribution of the difference of the cluster positions on each projection between MM 3 and 4 for the same track candidate in an event. The distribution has a flat background with less than 2% of the events with a difference larger than $4\sigma_{MM}$, where σ_{MM} is the standard deviation of the distribution ∼400 μm for the deflected beam. The resolution is limited mainly by the energy spread of the selected track. Systematic uncertainties due to orientation of the MM modules (along the rotational axes) are not taken into account for this estimation. The estimation gives an upper limit to the level of

wrong cluster identification after the cleaning method to resolve the multiplexing ambiguities. Thus we present an efficient way to limit the level of ambiguity decreasing substantially, from ∼50% to <2%, the chance of wrong cluster identification using the cluster size and integrated charge information as well as the channel number. With higher flux and pile up one can reduce the factor of multiplexing to limit the level of ambiguity further, depending on the acceptable level of ambiguities for the respective applications. One can also adapt the mapping of the channels to reduce the probability of "ghost" clusters due to the charge spread of clusters spanning over k strips, where k is the average size of the clusters for the given application. However, further studies with larger detectors and different multiplexing factors tested in higher flux environment, and comparison of their performance with non-multiplexed modules, are required to establish the extension of these modules to larger scale systems.

3.5. Time calculation

The timing calculation is based on the method used for the GEM detectors in the COMPASS experiment [26]. The hit on a strip is defined when the third of the three analog samples from the APV25 chip (A0, A1, A2) is at least three standard deviations above the mean pedestal level. The latency between the trigger and the signal window is adjusted such that the three samples sit on the rising edge of the signal pulse as shown in Fig. 7. A scan between ± 75 ns (three time sample units) with respect to the original latency setting was used to determine the rising edge. To calculate the hit time for each strip and thus the time of the signal cluster, one defines the ratios

$$r_{02} = \frac{A0}{A2} \quad \text{and} \quad r_{12} = \frac{A1}{A2} \tag{3}$$

that can be described by the function [27]

$$r(t) = \frac{r_0}{(1 + \exp(\frac{t-t_0}{\tau}))} \tag{4}$$

where r is either r_{02} or r_{12}.

The three parameters t_0, r_0 and the slope τ along-with the covariance matrix are found by fitting with Eq. (4) the latency scan (Fig. 8).

The strip hit time can thus be calculated with

$$t(r) = t_0 + \tau \ln(\frac{r_0}{r} - 1). \tag{5}$$

The uncertainty on the ratios is given by:

$$\sigma_{r_{02,12}} = (\sigma_i + \frac{1}{\sqrt{12}})\frac{\sqrt{A(0,1)^2 + A2^2}}{A2^2} \tag{6}$$

σ_i is the standard deviation of the pedestal of the ith channel reading the strip in the signal cluster. The additional $1/\sqrt{12}$ factor comes from the standard deviation of a standard uniform distribution on the strip connected to the channel.

The calculations give two times per hit strip, t_{02}^i and t_{12}^i, from the two ratios r_{02}^i and r_{12}^i with the corresponding parameters and errors for the ith strip in the cluster. The errors on the individual ratio's time $\sigma_{t_{02,12}}^i$ (for the ith strip) is calculated for all hit strips in the cluster and the cluster time is calculated as

$$t = \frac{\Sigma_{i=0}^{n}(\frac{(t_{02}^i)}{(\sigma_{t_{02}}^i)^2} + \frac{(t_{12}^i)}{(\sigma_{t_{12}}^i)^2})}{\Sigma_{i=0}^{n}(\frac{1}{(\sigma_{t_{02}}^i)^2} + \frac{1}{(\sigma_{t_{12}}^i)^2})} \tag{7}$$

where n is the number of strips in the event cluster.

4. Detector performance

The Micromegas gain was characterized with a radioactive source and then the modules were tested during the beam time of NA64 in October 2016 at CERN. During the four weeks beam run the performance of
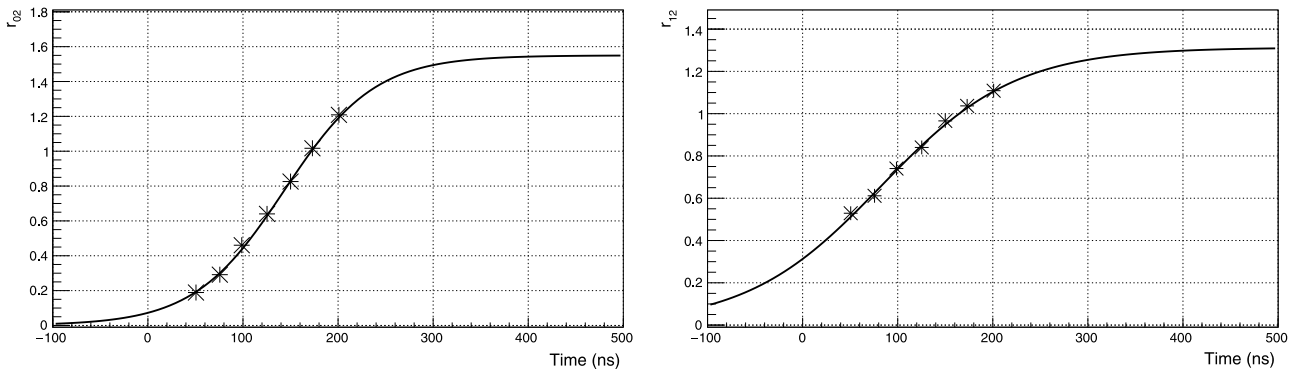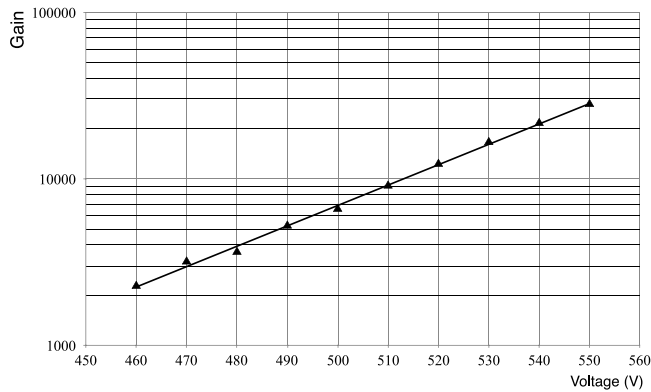
Fig. 8. Ratio r_{02} and r_{12} as a function of the latency settings.

Fig. 9. Gain of a Micromegas module as a function of the amplification voltage.

Fig. 11. Hit detection efficiency of the four MM modules as a function of the beam flux.
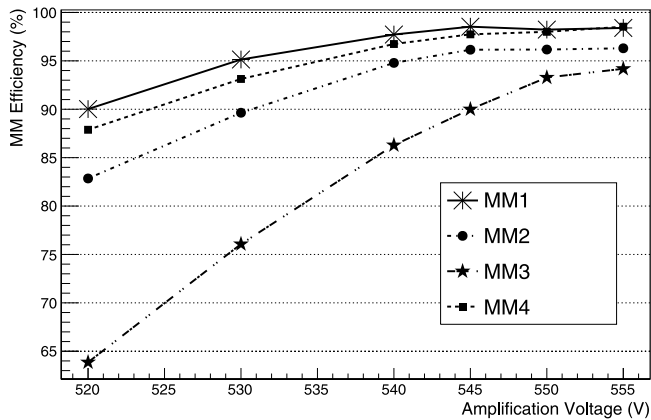

Fig. 10. Hit detection efficiency of the four MM modules as a function of the amplification voltage.

these multiplexed modules were checked for different beam intensities to establish their efficiency in a high flux beam. The clustering algorithm for the multiplexed detectors, described above, was included in the data analysis.

4.1. Characterization and gain

The Micromegas detectors were first characterized with a radioactive ^{55}Fe source to measure their gain. The gain, G, is defined as the total number of electrons produced after amplification, per single incident electron in the gas volume as G $= \frac{N_{total}}{N_{prim}}$, where N_{prim} is the
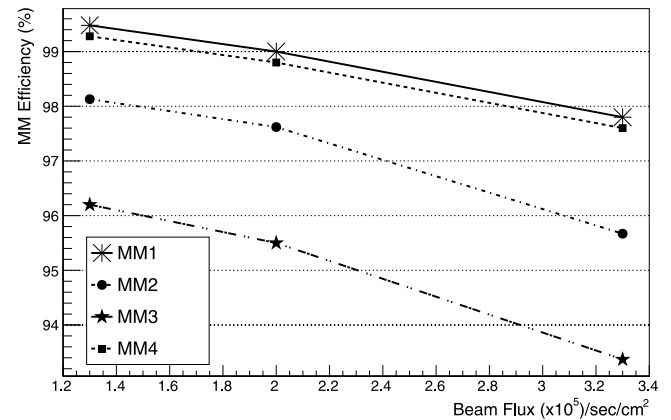
number of electrons liberated by the ionization of Argon in the drift region and N_{total} is the total number of electrons after the amplification. The number of primary electrons is directly related to the nature of the gas and the energy of the incoming particle, $E_x = 5.9$ keV for ^{55}Fe, as $N_{prim} = \frac{E_x}{\omega_i} = 223$ e$^-$, where $\omega_i = 26.5$ eV/e$^-$ is the ionization potential of Ar–CO$_2$ (93%–7%) [28]. So the gain of each detector was calculated by measuring the total current on the strips taking into account the rate of interactions. The drift electrode and the R-strips were connected to a high voltage of polarity negative and positive respectively through a RC filter and the mesh was grounded. The drift voltage was fixed at -300 V and the amplification voltage was applied on the R-strips starting from $+460$ V. The gain obtained as a function of the amplification voltage is shown in Fig. 9 for one module (MM1) as an example. The amplification voltage was kept below the spontaneous breakdown voltage limit of 560–570 V and the typical gain is about 3×10^4 at a amplification voltage $\sim$550 V. Detailed reasoning of breakdown mechanisms in gas detectors is presented in [29].

4.2. Hit detection efficiency

The hit detection efficiency, defined as the fraction of events with at least one signal cluster (on both X and Y plane) with respect to the triggered events, was measured in the beam, as a function of the amplification voltage as shown in Fig. 10. The Micromegas detectors were placed in the maximal beam intensity of 3.3×10^5 e$^-$/(s cm^2). The efficiency for all four modules increases with increasing voltage, as expected with the increase of the gain, and saturates at around 545 V. The Micromegas efficiency was also checked for different beam fluxes after fixing the amplification voltage at $\sim$555 V for MM 2, 3 and 4 and $\sim$545 V for MM 1, those being the voltages at which the respective
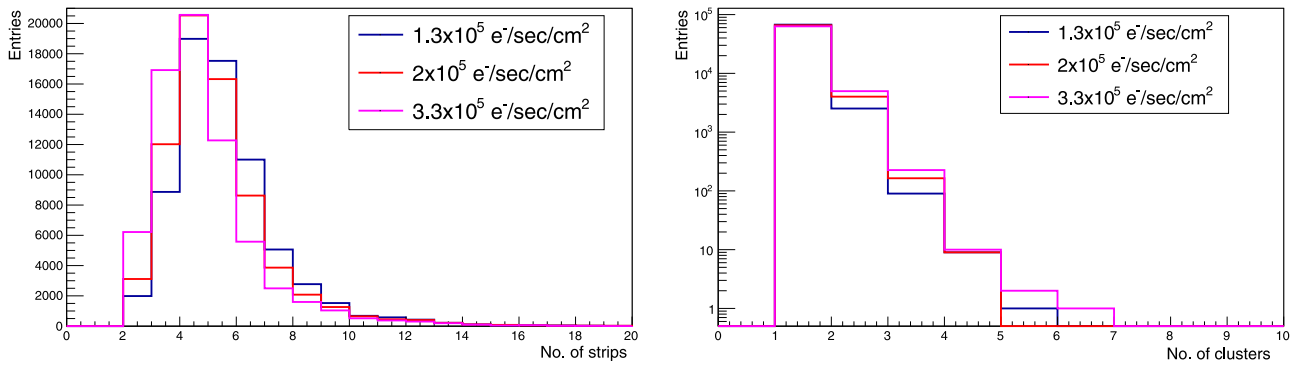
Fig. 12. Size of clusters (left) and No. of clusters per event (right) as a function of the beam flux.
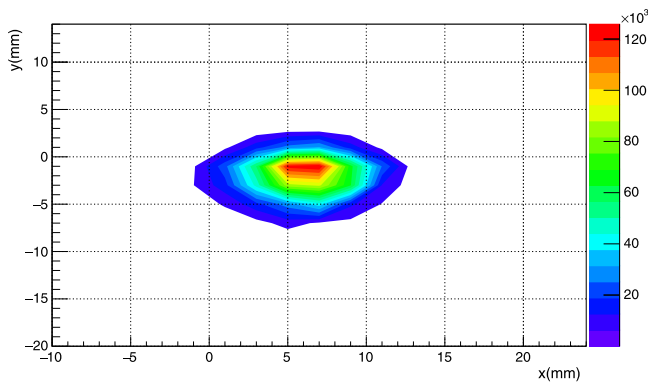

Fig. 13. Typical beam spot on the four Micromegas modules.

modules were most hit efficient. Fig. 11 shows the efficiency of the MM modules as a function of the beam flux. As one can see, for the maximal rate, the average hit detection efficiency of the four MM modules is ~96% with MM3 being the least efficient. It was found to be the most noisy detector from the pedestal distribution (larger pedestal standard deviation) of its electronic channels.

Fig. 12 (left) shows the distribution of the cluster size on one plane (X) and (right) the number of clusters per event as a function of the beam flux. As seen, the cluster size distribution barely changes indicating that the multiplexing is not responsible for the efficiency drop observed

at higher fluxes. This effect is related to the increase of pileup events and detector discharges as was observed during the particle spill with increasing flux.

4.3. Spatial resolution

The spatial resolution of these modules was measured in the beam at the highest beam intensity. Fig. 13 shows the typical beam spot on the MM modules. The distribution of the difference between the signal cluster positions of the undeflected beam (without the magnetic field) on the MM modules is shown in Fig. 14. The standard deviation of the distribution is a convolution of the spatial resolution of the two chambers. If we assume a parallel beam and that the two chambers have the same spatial resolution, σ, for a single chamber the resolution can be estimated to be $\sigma = \sigma_d/\sqrt{2} \sim 100$ μm (σ_d is the standard deviation of the distribution). Uncertainties due to the beam divergence and relative misalignment between detector modules and rotation of the modules with respect to the beam axis was not taken into account for this estimation. In order to establish that the multiplexing does not limit the resolution of the modules, the resolution of non-multiplexed Micromegas modules of same strip pitch was also checked similar to the multiplexed modules. Fig. 15 shows the distribution of the difference between the signal cluster positions between two non-multiplexed modules. The resolution obtained ~100 μm is comparable to that of the multiplexed detectors. This shows that the modules not only are efficient but also have good hit resolution under such high intensities.

Fig. 16 shows the time distribution of each plane with respect to the time of scintillator S1. The resolution obtained is $\sigma_t \sim 15$ ns. The
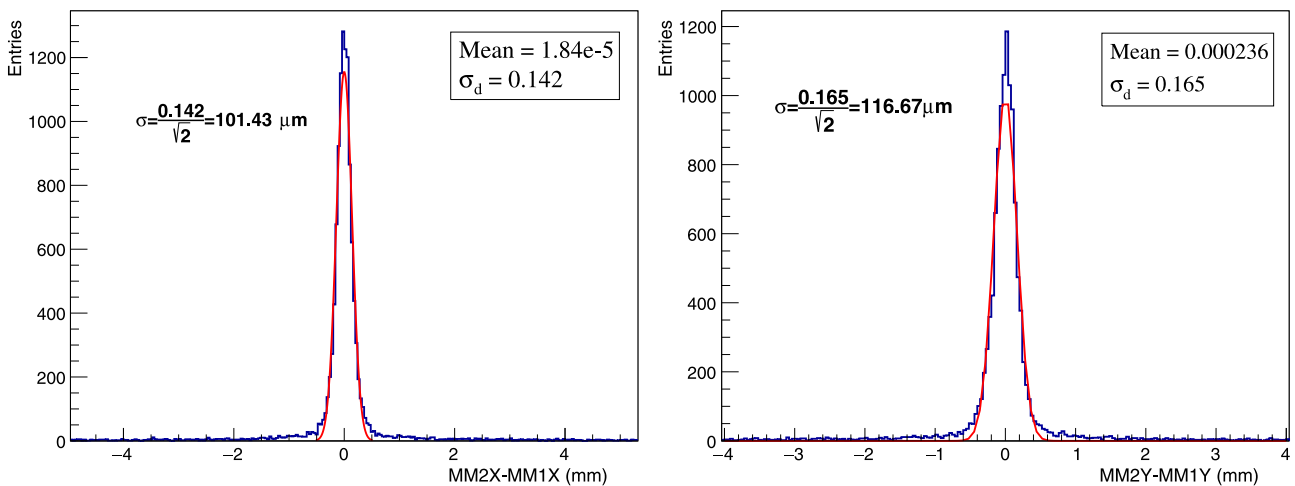

Fig. 14. Distribution of difference of cluster positions in each projection between two MM modules. The black histogram is the data and the red line is a fitted Gaussian function with parameters "σ_d" and "Mean". Assuming the same spatial resolution for the two modules the fit gives a position resolution ~100 μm for each module. (For interpretation of the references to color in this figure legend, the reader is referred to the web version of this article.)
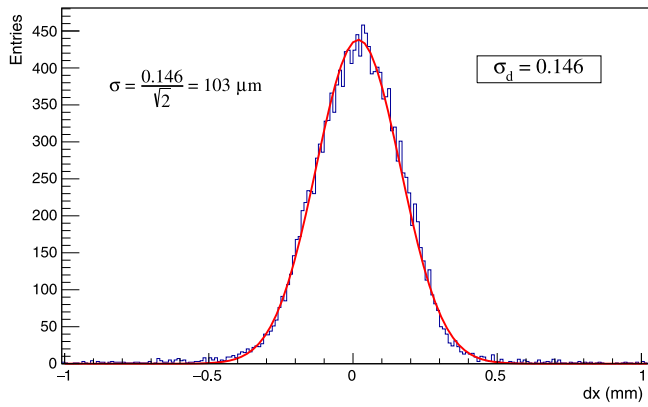
Fig. 15. Distribution of difference of cluster positions for one projection between two non-multiplexed MM modules. The blue histogram is the data and the red line is a fitted Gaussian function with parameters "σ_d". Assuming the same spatial resolution for the two modules the fit gives a position resolution ~100 μm for each module. (For interpretation of the references to color in this figure legend, the reader is referred to the web version of this article.)
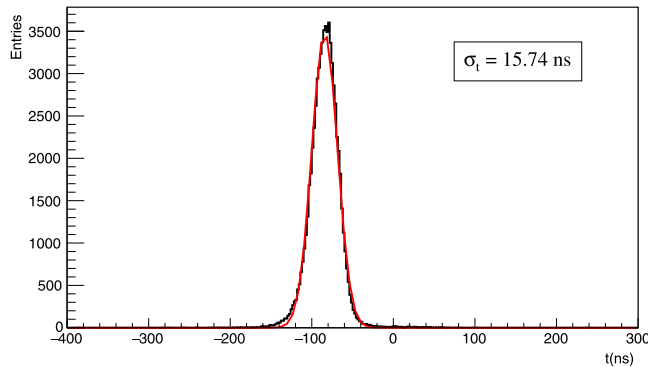
Fig. 16. Timing distribution of the Micromegas modules with respect to scintillator S1 time. The black histogram is data and the red line is a fitted Gaussian function with standard deviation σ_t. (For interpretation of the references to color in this figure legend, the reader is referred to the web version of this article.)

MAMMA collaboration tested Micromegas modules for the ATLAS New Small Wheel upgrade with APV chips sampling the entire signal shape and reported a resolution <10 ns in their test beam [30]. Therefore, it should be possible to improve our timing, sampling the entire signal shape instead of just three samples as mentioned in Section 3.4. The distribution of the size of clusters/plane is shown in Fig. 17 in units of number of strips. The difference in the cluster size in the X and Y plane is expected due to the fact that the charge spreading along the R-strips crosses several Y strips.
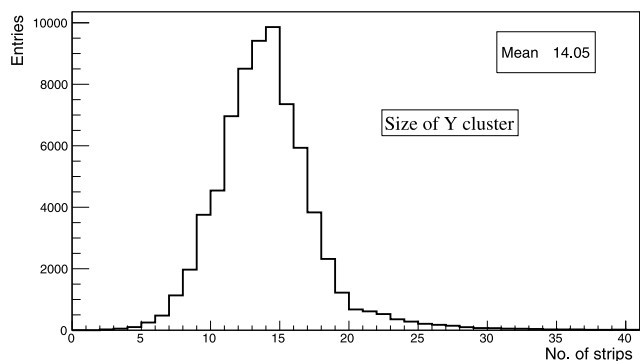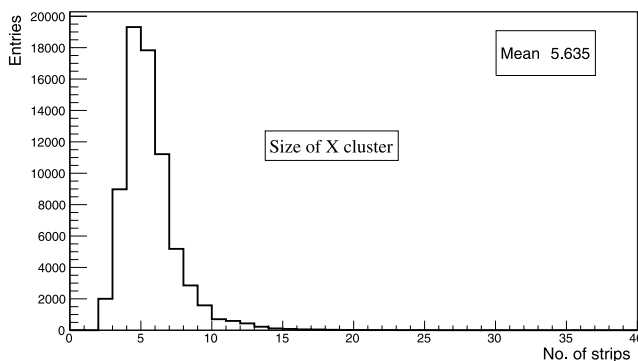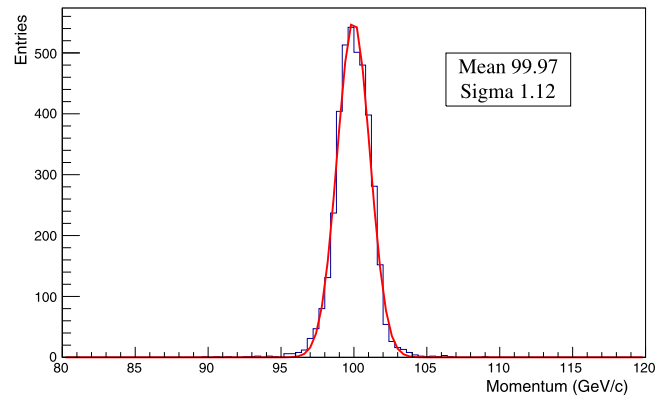

Fig. 18. Reconstructed momentum with the four Micromegas modules for a 100 GeV/c beam. The black histogram is data and the red line is a fitted Gaussian function with parameters "Sigma" and "Mean". (For interpretation of the references to color in this figure legend, the reader is referred to the web version of this article.)

4.4. Tracking in NA64 and suppression of low energy electron tail

The multiplexed modules were built for tracking in the NA64 experiment to suppress the low energy electron tail as mentioned above. Tracking of the incoming particles with the four modules was done under an integrated magnetic field of 7 T.m over two magnets with a combined length of 4.8 m as shown in Fig. 1. The deflection at the point of MM3 and MM4 for a 100 GeV/c beam was ~31.5 cm and 35 cm respectively. Fig. 18 shows the reconstructed momentum for a 100 GeV/c electron beam as obtained with the Genfit software (a generic track reconstruction framework for nuclear and particle physics [31]). The resolution of the central peak is ~1.1% as shown in the plot with an efficiency of 85%. To improve the tracking efficiency, the number of MM stations that will be used in the next NA64 beam time will be doubled, i.e. four MM's will be placed before and four after the bending magnets. This upgrade will result in an increased overall efficiency of 92%.

The preparation of a collinear beam is a key point in NA64. The MM were used to precisely measure the incoming angle of the particles in order to tune and optimize the beam collinearity. The angle was determined with an accuracy better than 1 mrad allowing to reject large angle tracks and keeping the divergence of the beam within 1 mrad as shown in Fig. 19. This accuracy allows to use the MM also for the transversal scan of the ECAL hermeticity in order to look for non-uniformities.

In NA64 the trigger of the experiment is received from scintillators S1–S3 ~3 cm in diameter. Therefore, the acceptance of the trigger alone should select the incoming beam energy to a precision ~±5 GeV, unless they enter with a large incident angle with respect to the

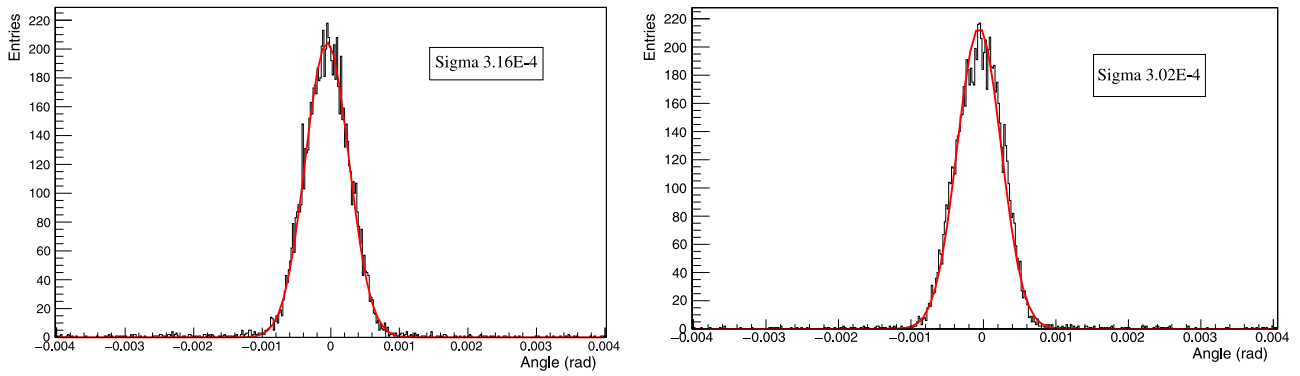**Fig. 17.** Cluster size per plane in the Micromegas modules.

Fig. 19. Left: incoming particle azimuthal angle before the spectrometer measured with MM1 and MM2 with respect to the average beam axis. Right: outgoing particle azimuthal angle measured after the magnets with MM3 and MM4 with respect to the average deflected beam axis.
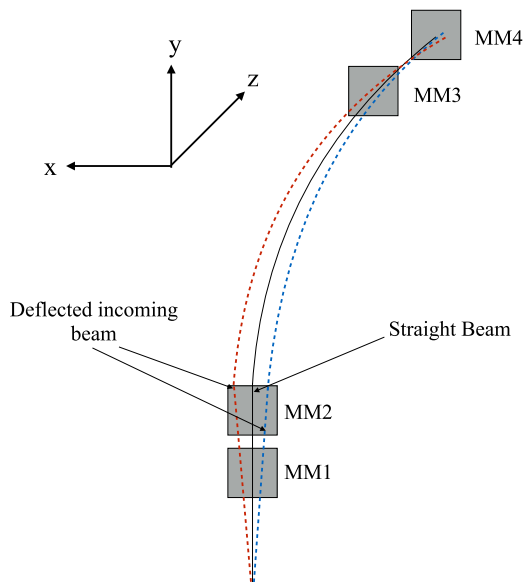

Fig. 20. Example of incoming beam deflection. Incoming angle is calculated with respect to the Z-axis.

with increasing angle. Therefore, the incoming angle measured by the two MMs (MM1, MM2 in Fig. 1) upstream the magnet is a powerful tool to reject low energy electrons that are a dangerous background for the experiment [15].

5. Conclusion

This paper presents the first results of Multiplexed Resistive XY Micromegas modules in a high flux beam performing with an average hit efficiency of 96% per module for a multiplexing factor of five. Multiplexed detectors are a novel idea to reduce the number of readout channels which can be very useful for the need of particle physics experiments to cover large areas without compromising single hit resolution to perform precise tracking with reduced cost. So far the Multiplexed Resistive XY Micromegas modules have only been tested experimentally using cosmic rays [32] for muon tomography studies with Micromegas based telescopes. Our work is the first to report on the performance of these detectors in a high flux beam environment. However, with multiplexing any grouping implies a certain loss of information. This is the reason why ambiguities can occur due to "ghost" signals from fake combinations. Our measurements show that it is indeed possible to limit the ambiguities using information from cluster size, integrated charge as well as the channel number with <2% chance of wrong cluster identification, thus allowing for an efficient and reduced-cost tracking detector to a high rate environment. Further studies with larger multiplexed detectors in higher flux environment are required to establish the performance and extension of this technology for larger scale tracking. In this study we showed that the multiplexed technology can be used in NA64, with a tracking resolution of 1.1% obtained for a 100 GeV/c beam.

primary beam direction. The reconstructed momentum was, therefore, checked as a function of the incoming beam angle for all triggered events. Fig. 20 shows a sketch of the incoming beam. The angle of the incoming beam with respect to the z-axis was calculated from the MM1 and 2 hit positions and the reconstructed momentum was plotted as a function of the angle as shown in Fig. 21. As expected, when the initial deflection is in the negative x direction the reconstructed momentum is larger with increasing angle and when the initial deflection is in the positive x direction the reconstructed momentum tends to be smaller
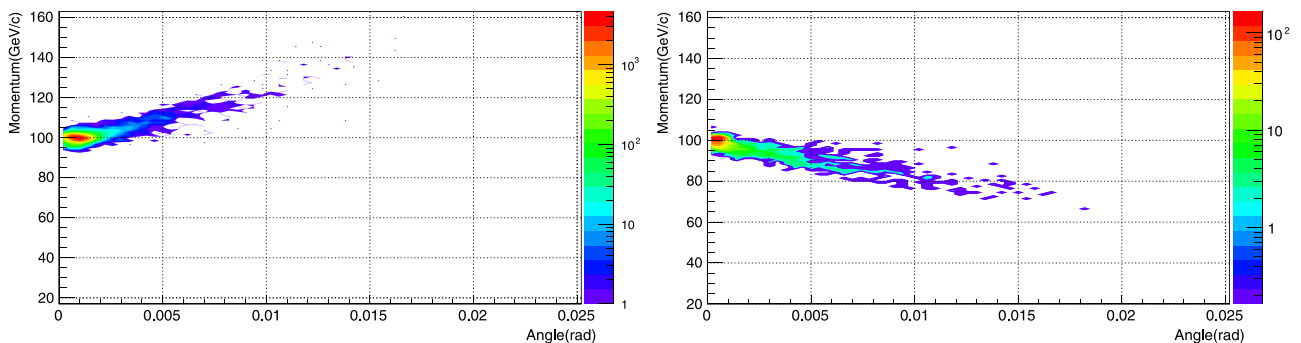

Fig. 21. Momentum reconstructed as a function of the incoming angle for incoming particle deflected towards the negative *x* axis (left) and positive *x* axis (right).

References

[1] B. Beltran, et al., Search for solar axions: The CAST experiment at CERN, Nucl. Instr. and Meth. in Phys. Res. B 197 (2005) 62–65.

[2] Y. Giomataris, Ph. Rebourgeard, J.P. Robert, G. Charpak, Nucl. Instr. and Meth. in Phys. Res. A 376 (1996) 29–35.

[3] COMPASS Collaboration, COMPASS experiment at CERN, Nucl. Instr. and Meth. in Phys. Res. A 577 (2007) 455–518.

[4] Gabriel Charles, Development of Micromegas detectors for the CLAS12 experiment at Jefferson Laboratory, (FRCEA-TH-5915), September 2013.

[5] F.J. Iguaz, D. Attie, D. Calvet, et al., Micromegas detector developments for dark matter directional detection with MIMAC, Journal of Instrumentation 6 (2011).

[6] J. Derre, Y. Giomataris, H. Zaccone, A. Bay, J.P. Perroud, F. Ronga, Nucl. Instrum. Meth. A 459 (2001) 523. http://dx.doi.org/10.1016/S0168-9002(00)01051-2.

[7] A. Peyaud, A. Angelopoulos, C. Chelmis, et al., The forfire photodetector, Nucl. Instr. and Meth. in Phys. Res A 787 (2015) 102–104.

[8] Maxim Titov, Perspectives of micro-pattern gaseous detector technologies for future physics projects, 2013. arXiv:1308.3047.

[9] T. Alexopoulos, et al., Nucl. Instr. Meth. Phys. Res. A 640 (2011) 110–118.

[10] M. Byszewski, J. Wotschack, Resistive-strips Micromegas detectors with two-dimensional readout, JINST 7 (2012) C02060.

[11] S. Procureur, R. Dupre, S. Aune, Genetic multiplexing and first results with a 50×50 cm^2 Micromegas, Nucl. Instr. and Meth. in Phys. Res. A 729 (2013) 888–894.

[12] Bin-Xiang Qi, Shu-Bin Liu, et al., A novel method of encoded multiplexing readout for micro-pattern gas detectors, 2015. arXiv:1509.02229.

[13] S. Andreas, D. Banerjee, S.V. Donskov, P. Crivelli, A. Gardikiotis, S.N. Gninenko, F. Guber, Proposal for an experiment to search for light dark matter at the SPS, 2013. arXiv:1312.3309.

[14] J.L. Hewett, arXiv:1205.2671.

[15] D. Banerjee, et al., NA64 Collaboration, Search for invisible decays of sub-GeV dark photons in missing-energy events at the CERN SPS, Phys. Rev. Lett. 118 (2017) 011802.

[16] http://sba.web.cern.ch/sba/ and http://nahandbook.web.cern.ch/.

[17] E. Depero, D. Banerjee, et al., High purity 100 GeV electron identification with synchrotron radiation, 2017. arXiv:1703.05993, accepted for publication in Nucl. Instr. and Meth. A.

[18] D. Banerjee, P. Crivelli, A. Rubbia, Beam purity for light dark matter search in beam dump experiment, Adv. High Energy Phys. (2015) 105730.

[19] A.J.P.L. Policarpo, Physica Scripta 23 (1981) 539.

[20] R.C. Weast, Handbook of Chemistry and Physics, C.R.C. Press, Bica Raton, FL, 1981, p. 205.

[21] R.I. Schoen, J. Chem. Phys. 17 (1962) 2032.

[22] Yu.N. Pestov, et al., Nucl. Instr. and Meth. A 456 (2000) 11.

[23] M.J. French, L.L. Jones, et al., Design and results from the APV25, a deep sub-micron CMOS front-end chip for the CMS tracker, Nucl. Instr. and Meth. in Phys. Res. A 466 (2001) 359–365.

[24] B. Ketzer, S. Bachmann, et al., GEM detectors for COMPASS, IEEE Trans. Nucl. Sci. 48 (4) (2001).

[25] https://wwwcompass.cern.ch/compass/detector/daq/status/daqdoc.html.

[26] Sebastian Uhl, Diploma thesis, construction and commissioning of the pixelGEM tracking system for the COMPASS Experiment, 2008.

[27] Q. Weitzel, Triple GEM detectors in COMPASS - a performance study. Diploma thesis, Technische Universität München, November 2003.

[28] Maxim Titov, Gaseous detectors: Recent developments and applications, 2010. arXiv:1008.3736.

[29] A. Bressan, M. Hoch, P. Pagano, et al., High rate behavior and discharge limits in micro-pattern detectors, Nucl. Instr. and Meth. in Phys. Res. A 424 (1999) 321–342.

[30] Y. Kataoka, et al., Performance studies of a Micromegas chamber in the ATLAS environment, JINST 9 (2014) C03016.

[31] C. Höppner, S. Neubert, B. Ketzer, et al., Nucl. Instr. and Meth. in Phys. Res. A 620 (2010) 518–525.

[32] S. Bouteille, D. Attie, P. Baron, D. Calvet, P. Magnier, et al., A Micromegas-based telescope for muon tomography, Nucl. Instr. and Meth. in Phys. Res. A 834 (2016) 223–228.